Determination of the Fe−Ligand Bond Lengths and Fe−N−O Bond Angles in Horse Heart Ferric and Ferrous Nitrosylmyoglobin Using Multiple-Scattering XAFS Analyses

Anne M. Rich, Robert S. Armstrong,* Paul J. Ellis, and Peter A. Lay*

Contribution from the School of Chemistry, University of Sydney, New South Wales 2006, Australia

Received January 22, 1998

Abstract: The structural characterizations of the Fe environments in the NO adducts of horse heart ferric (Fe^{III}) and ferrous (Fe^{II}) nitrosylmyoglobin (MbNO) have been achieved by multiple-scattering (MS) analyses of XAFS data obtained from frozen aqueous solutions. For $Mb^{II}NO$, the MS analysis resulted in an averaged Fe−N_p (pyrrole) distance of 2.00 Å, an Fe−N_ϵ (imidazole) distance of 2.05 Å, an Fe−N_{NO} distance of 1.75 Å, and an Fe−N−O angle of 150°. For comparison, the MS analysis of the XAFS data of [Fe^{II}(TPP)(NO)] (TPP = tetraphenylporphyrinato) resulted in bond lengths of 2.01 Å for Fe−N_p and 1.74 Å for Fe−N_{NO} and an Fe−N−O bond angle of 155°. The Fe−N_{NO} and N−O distances obtained from the analysis of $Mb^{II}NO$ are in good agreement with those determined crystallographically for [Fe^{II}(TPP)(NO)] with and without 1-methylimidazole (1-MeIm) as the sixth ligand. The MS analysis of $Mb^{III}NO$ yielded an average Fe−N_p distance of 2.00 Å, an Fe−N_ϵ distance of 2.04 Å, an Fe−N_{NO} distance of 1.69 Å, and an Fe−N−O angle of 180°. These bond lengths and angles are consistent with the crystal structures of model complexes [Fe^{III}(TPP)(NO)(OH_2)]$^+$ and [Fe^{III}(OEP)(NO)]$^+$ (OEP = octaethylporphyrinato). The final XAFS *R* values were 14.5, 14.6, and 12.7% for $Mb^{III}NO$, $Mb^{II}NO$, and [Fe^{II}(TPP)(NO)], respectively.

Introduction

The monoheme protein myoglobin (Mb) consists of a single polypeptide chain of 153 amino acid residues covalently bound through an imidazole of the proximal histidine to an Fe of protoporphyrin IX. In cardiac muscle it stores O_2 and facilitates its diffusion from blood capillaries to the mitochondria.[1] In vivo, it is maintained in the ferrous (Fe^{II}) state, being high-spin five-coordinate in deoxy-Mb and low-spin six-coordinate in oxy-Mb. In vitro, oxy-Mb is oxidized to the Fe(III) form, met-Mb, where the sixth ligand is water, which may be hydrogen bonded with the "distal" histidine.[2] Although there are structural sequence differences between sperm whale (SW) and horse heart (HH) Mb,[1,3] their overall protein structures, spectra, and reactivities are very similar.[2,4−15] The recently established biological relevance of NO binding to hemeproteins[16−21] has heightened interest in both the Fe(II) and Fe(III) adducts, which has led to the current study on the XAFS of the NO adducts of HH Mb. The results of this study are compared with literature information on the structures of NO adducts of SW and HH Mb derived from a range of techniques.

Nitric oxide is a secretory product of mammalian cells[22] and plays a role in a large range of physiological processes, including signal transmission, blood clotting, and blood pressure control, and has a role in the ability of the immune system to kill tumor cells and intracellular parasites.[16,18,22−31] Since the biological half-life of NO is short (∼5 s),[29] it is somewhat surprising that

(1) Evans, S. V.; Brayer, G. D. *J. Biol. Chem.* **1988**, *263*, 4263−4268.
(2) Antonini, E.; Brunori, M. *Hemoglobin and Myoglogin in Their Reactions with Ligands*; Neuberger, A., Tatum, E. L., Eds.; North-Holland: Amsterdam, 1971.
(3) Hauksson, J. B.; La Mar, G. N.; Pandey, R. K.; Rezzano, I. N.; Smith, K. M. *J. Am. Chem. Soc.* **1990**, *112*, 6198−6205.
(4) The two structures exhibit 87% sequence identity (133 out of 153 AA residues aligned).[5]
(5) Vinogradov, S. N.; Walz, D. A.; Pohajdak, B.; Moens, L.; Kapp, O. H.; Suzuki, T.; Trotman, C. N. A. *Comput. Biochem. Physiol. B* **1993**, *106B*, 1−26.
(6) Gibson, Q. H. *Biochem. J.* **1959**, *71*, 293−303.
(7) Antonini, E. *Physiol. Rev.* **1965**, *45*, 123−170.
(8) Rohlfs, R. J.; Olson, J. S.; Gibson, Q. H. *J. Biol. Chem.* **1988**, *263*, 1803−1813 and references therein.
(9) Rohlfs, R. J.; Mathews, A. J.; Carver, T. E.; Olson, J. S.; Springer, B. A.; Egeberg, K. D.; Sligar, S. G. *J. Biol. Chem.* **1990**, *265*, 3168−3176.
(10) Carver, T. E.; Olson, J. S.; Smerdon, S. J.; Krzywda, S.; Wilkinson, A. J.; Gibson, Q. H.; Blackmore, R. S.; Ropp, J. D.; Sligar, S. G. *Biochemistry* **1991**, *30*, 4697−4705.
(11) Carver, T. E.; Rohlfs, R. J.; Olson, J. S.; Gibson, Q. H.; Blackmore, R. S.; Springer, B. A.; Sligar, S. G. *J. Biol. Chem.* **1990**, *265*, 20007−20020.
(12) Quillin, M. L.; Arduini, R. M.; Olson, J. S.; Phillips, G. N., Jr. *J. Mol. Biol.* **1993**, *234*, 140−155.
(13) Springer, B. A.; Sligar, S. G.; Olson, J. S.; Phillips, G. N., Jr. *Chem. Rev.* **1994**, *94*, 699−714.
(14) Hanania, G. I. H.; Yeghiayan, A.; Cameron, B. F. *Biochem. J.* **1966**, *98*, 189−192.
(15) Scheler, W.; Schoffa, G.; Jung, F. *Biochem. Z.* **1957**, *329*, 232−246.
(16) Butler, A. R.; Williams, D. L. H. *Chem. Soc. Rev.* **1993**, *22*, 233−241.
(17) Das, T. K.; Mazumdar, S.; Mitra, S. *J. Chem. Soc., Chem. Commun.* **1993**, 1447−1448.
(18) Wang, J.; Stuehr, D. J.; Rousseau, D. L. *Biochemistry* **1997**, *36*, 4595−4606.
(19) Ignarro, L. J.; Ross, G.; Tillisch, J. *West. J. Med.* **1991**, *154*, 51−62.
(20) Lancaster Jr., J. R.; Langrehr, J. M.; Bergonia, H. A.; Murase, N.; Simmons, R. L.; Hoffman, R. A. *J. Biol. Chem.* **1992**, *267*, 10994−10998.
(21) Andersen, J. F.; Champagne, D. E.; Weichsel, A.; Ribeiro, J. M. C.; Balfour, C. A.; Dress, V.; Montfort, W. R. *Biochemistry* **1997**, *36*, 4423−4428.
(22) Xie, Q.-W.; Cho, H. J.; Calaycay, J.; Mumford, R. A.; Swiderek, K. M.; Lee, T. D.; Ding, A.; Troso, T.; Nathan, C. *Science (Washington, D.C.)* **1992**, *256*, 225−228.
(23) Verma, A.; Hirsch, D. J.; Glatt, C. E.; Ronnett, G. V.; Snyder, S. H. *Science (Washington, D.C.)* **1993**, *259*, 381−384.

10.1021/ja980253g CCC: $15.00
Published on Web 10/13/1998

it serves important and diverse biological functions.[32] Heme-proteins involved in these functions include nitric oxide synthases (NOSs), which oxidize arginine to citrulline with concomitant release of NO;[18,26,30,33] the human receptor for NO guanylate cyclase (sGC);[28,34−40] and nitrophorins in the saliva of the bloodsucking insect, *Rhodnius prolixus*, which bind and transport NO as the Fe(III) adduct into the host skin to cause vasodilation and facilitate feeding.[21,24,41] The essential role played by NO in the nervous and vascular systems is in sharp contrast to its high degree of toxicity that is associated with (1) coordination to, or oxidation of, the Fe^{II} in Hb to generate met-Hb, thereby decreasing the O_2-carrying capacity of the blood,[42] (2) binding to ferrous heme and iron−sulfur centers of enzymes, (3) hydroxyl radical formation, and (4) neurotoxicity arising from excessive concentrations of NO as a neuromodulator.[25] Hb serves as a buffer against NO toxicity, since it coordinates NO and NO precursors, such as hydroxylamine and nitrite, and minimizes NO penetration of the blood−brain barrier, thus protecting the central nervous system.[25] Despite their considerable physiological interest, very little structural information is available on NO adducts of heme proteins. The latter is confined to a single-scattering (SS) XAFS analysis of SW Mb^{II}-NO[43] (only average Fe−N bond lengths for the Fe−N_p and Fe−N_ϵ bonds were reported); the X-ray crystal structures of the NO adducts of horse Hb ($Hb^{II}NO$),[44] the plant heme, lupin Lb (Lb^{II}-NO),[45] and cytochrome *c* peroxidase;[46] and the MS XAFS analysis of the NO adduct of the ferric hemeprotein, nitric oxide reductase, from *Fusarium oxysporum*.[47] Very recently, an X-ray structure of the NO adduct of SW myoglobin ($Mb^{II}NO$) has also been reported.[48]

Many of the conclusions about the electronic structures of NO complexes and Fe−N−O angles in the Fe(II) adducts are also derived from the interpretation of EPR data.[49−57] A single-crystal EPR study of SW MbNO at 77 K[50,52] was used to estimate the Fe−N−O bond angle to be 108−110°, which was consistent with the bond angle determined by XRD (112°).[48] This is in contrast with the X-ray crystallographic study of horse HbNO, which indicated an Fe−N−O bond angle of 145 ± 10°.[44] From these observations, Hori et al.[53] suggested that the metal−ligand geometry in MbNO and HbNO may be different in solutions and crystals. Phillips also noted that the angle in the crystals of $Mb^{II}NO$ may be influenced by the crystal structure of met-Mb, since the crystals of $Mb^{II}NO$ were grown by NO diffusion into met-Mb crystals, with subsequent autoreduction of the Fe(III) adduct.[48] Hori et al. have also postulated that the different EPR spectra of SW MbNO at 77 and 293 K resulted from a change in conformation of NO bonding upon freezing, i.e., at ambient temperature (293 K), the Fe−N−O bond angle was estimated to be 153°, and at 77 K, the Fe−N−O bond angle was estimated to be 109°.[53]

Another technique that has been used to obtain information about the electronic structures and the Fe−N−O bond angles in NO adducts of a range of hemeproteins (including Mb) is resonance Raman spectroscopy.[47,58−61] These results indicate a bent Fe−N−O moiety for the Fe(II) adduct and a linear Fe−N−O moiety with an $Fe(II)-NO^+$ electronic structure for the Fe(III) adduct.

Studies on MbNO adducts have direct relevance to the transport and detoxification of NO as well as serving as models for NO binding to a range of hemeproteins. For instance, it has been proposed that Fe(III) hemeproteins act as NO carriers[24] since they release NO more readily than do Fe(II) hemeproteins.[8,62] Such species are also intermediates in the reduction of nitrite by nitrite reductase.[63] MS analyses of XAFS data have been used successfully to determine Fe−N−O bond angles in non-heme Fe complexes[64] and the ferric hemeprotein nitric oxide reductase.[47] Hence, MS XAFS analyses have been undertaken in an attempt to delineate the apparently contradictory informa-

(24) Ribeiro, J. M. C.; Hazzard, J. M. H.; Nussenzveig, R. H.; Champagne, D. E.; Walker, F. A. *Science (Washington, D.C.)* **1993**, *260*, 539−541.
(25) Clarke, M. J.; Gaul, J. B. *Struct. Bonding* **1993**, *81*, 147−181 and references therein.
(26) Bredt, D. S.; Hwang, P. M.; Glatt, C. E.; Lowenstein, C.; Reed, R. R.; Snyder, S. H. *Nature (London)* **1991**, *351*, 714−718.
(27) Eich, R. F.; Li, T.; Lemon, D. D.; Doherty, D. H.; Curry, S. R.; Aitken, J. F.; Mathews, A. J.; Johnson, K. A.; Smith, R. D.; Phillips, G. N., Jr.; Olson, J. S. *Biochemistry* **1996**, *35*, 6976−6983.
(28) Stone, J. R.; Marletta, M. A. *Biochemistry* **1996**, *35*, 1093−1099 and references therein.
(29) Snyder, S. H. *Science (Washington, D.C.)* **1992**, *257*, 494−496.
(30) Bredt, D. S.; Hwang, P. M.; Snyder, S. H. *Nature (London)* **1990**, *347*, 768−770.
(31) Fukuto, J. M.; Ignarro, L. J. *Acc. Chem. Res.* **1997**, *30*, 149−152.
(32) Snyder, S. H.; Bredt, D. S. *Sci. Am.* **1992**, *266*, 28−35.
(33) Wang, J.; Rousseau, D. L.; Abu-Soud, H. M.; Stuehr, D. J. *Proc. Natl. Acad. Sci. U.S.A.* **1994**, *91*, 10512−10516 and references therein.
(34) Smith, R. P.; Louis, C. A.; Kruszyna, R. T.; Kruszyna, H. *Fundam. Appl. Toxicol.* **1991**, *17*, 120−127.
(35) Kim, S.; Deinum, G.; Gardner, M. T.; Marletta, M. A.; Babcock, G. T. *J. Am. Chem. Soc.* **1996**, *118*, 8769−8770.
(36) Stone, J. R.; Marletta, M. A. *Biochemistry* **1995**, *34*, 14668−14674.
(37) Stone, J. R.; Marletta, M. A. *Biochemistry* **1994**, *33*, 5636−5640.
(38) Ignarro, L. J.; Degnan, J. N.; Baricos, W. H.; Kadowitz, P. J.; Wolin, M. S. *Biochim. Biophys. Acta* **1982**, *718*, 49−59.
(39) Ignarro, L. J.; Wood, K. S.; Wolin, M. S. *Adv. Cyclic Nucleotide Protein Phosphorylation Res.* **1984**, *17*, 267−274.
(40) Ignarro, L. J. *Semin. Hematol.* **1989**, *26*, 63−76.
(41) Traylor, T. G.; Sharma, V. S. *Biochemistry* **1992**, *31*, 2847−2849.
(42) Addison, A. W.; Stephanos, J. J. *Biochemistry* **1986**, *25*, 4104−4113.
(43) Zhang, K.; Reddy, K. S.; Bunker, G.; Chance, B. *Proteins: Struct. Funct. Genet.* **1991**, *10*, 279−286.
(44) Deatherage, J. F.; Moffat, K. *J. Mol. Biol.* **1979**, *134*, 401−417.
(45) (a) Obmolova, G. V.; Safonova, T. N.; Teplyakov, A. V.; Popov, A. N.; Kuranova, I. P.; Harutyunyan, E. G.; Vainshtein, B. K. *Bioorg. Khim.* **1988**, *14*, 1509−1519. (b) Harutyunyan, E. H.; Safonova, T. N.; Kuranova, I. P.; Popov, A. N.; Teplyakov, A. V.; Obmolova, G. V.; Vainshtein, B. K.; Dodson, G. G.; Wilson, J. C. *J. Mol. Biol.* **1996**, *264*, 152−161.
(46) Edwards, S. L.; Poulos, T. L. *J. Mol. Biol.* **1990**, *265*, 2588−2595.
(47) Obayaashi, E.; Tsukamoto, K.; Adachi, S.-i.; Takahashi, S.; Nomura, M.; Iizuka, T.; Shoun, H.; Shiro, Y. *J. Am. Chem. Soc.* **1997**, *119*, 7807−7816.
(48) Brucker, E. A.; Olson, J. S.; Ikeda-Saito, M.; Phillips, G. N., Jr. *Proteins: Struct. Funct. Genet.* **1998**, *30*, 352−356.
(49) Maskall, C. S.; Gibson, J. F.; Dart, P. J. *Biochem. J.* **1977**, *167*, 435−445.
(50) Chien, J. C. W. *J. Chem. Phys.* **1969**, *51*, 4220−4227.
(51) Stone, J. R.; Sands, R. H.; Dunham, W. R.; Marletta, M. A. *Biochem. Biophys. Res. Commun.* **1995**, *207*, 572−577.
(52) Dickinson, L. C.; Chien, J. C. W. *J. Am. Chem. Soc.* **1971**, *93*, 5036−5040.
(53) Hori, H.; Ikeda-Saito, M.; Yonetani, T. *J. Biol. Chem.* **1981**, *256*, 7849−7855.
(54) Morse, R. H.; Chan, S. I. *J. Biol. Chem.* **1980**, *255*, 7876−7882.
(55) O'Keeffe, D. H.; Ebel, R. E.; Peterson, J. A. *J. Biol. Chem.* **1978**, *253*, 3509−3516.
(56) Waleh, A.; Ho, N.; Chantranupong, L.; Loew, G. H. *J. Am. Chem. Soc.* **1989**, *111*, 2767−2772.
(57) Henry, Y.; Banerjee, R. *J. Mol. Biol.* **1973**, *73*, 469−482.
(58) Benko, B.; Yu, N.-T. *Proc. Natl. Acad. Sci. U.S.A.* **1983**, *80*, 7042−7046.
(59) Walters, M. A.; Spiro, T. G. *Biochemistry* **1982**, *21*, 6989−6995.
(60) Spiro, T. G.; Strekas, T. C. *J. Am. Chem. Soc.* **1974**, *96*, 338−345; Choi, S.; Spiro, T. G. *J. Am. Chem. Soc.* **1983**, *105*, 3683−3692; Owens, J. W.; O'Connor, C. J. *Coord. Chem. Rev.* **1988**, *84*, 1−45.
(61) Stong, J. D.; Burke, J. M.; Daly, P.; Wright, P.; Spiro, T. G. *J. Am. Chem. Soc.* **1980**, *102*, 5815−5819. Rich, A. M. BSc(Hons) Thesis, University of Sydney, 1990.
(62) Sharma, V. S.; Traylor, T. G.; Gardiner, R.; Mizukami, H. *Biochemistry* **1987**, *26*, 3837−3843.
(63) Wang, Y.; Averill, B. A. *J. Am. Chem. Soc.* **1996**, *118*, 3972−3973.
(64) Westre, T. E.; Cicco, A. D.; Filipponi, A.; Natoli, C. R.; Hedman, B.; Solomon, E. I.; Hodgson, K. O. *J. Am. Chem. Soc.* **1994**, *116*, 6757−6768.

tion on the Fe−N−O bond angles in the Fe(II) adducts of hemeproteins obtained from EPR spectroscopy and XRD and to provide the first direct structural evidence for this angle in the NO adduct of met-Mb. Moreover, the errors in bond lengths and angles in X-ray crystallography are large, even for high-resolution structures (typically ≥0.1 Å in bond lengths),[65] and hence, MS XAFS analyses have the potential to provide more accurate and precise Fe−L bond length data than those available from X-ray crystallography.

Experimental Section

All manipulations during the preparation of the deoxy-Mb and the NO adducts of Mb were performed using syringe techniques in an Ar-filled glovebag. A $Mb^{III}NO$ solution (4.6 mM) was prepared[66] by passing NO over the HH met-Mb (Sigma) solution (deoxygenated with Ar) for 5 min. Glycerol was deoxygenated with Ar, then NO was bubbled into the glycerol prior to mixing with a solution of $Mb^{III}NO$ in a sealed vial to give a 40% v/v glycerol/water solution. A glycerol solution of $Mb^{II}NO$ (3.8 mM) was prepared by forming the $Mb^{III}NO$ adduct (as above) and leaving the solution at 4 °C for 24 h to "autoreduce" to $Mb^{II}NO$,[41,62,67] prior to the addition of glycerol. The purities of the NO adducts were determined immediately prior to freezing by UV/vis spectroscopy[41] using a Hewlett-Packard 8452A diode array spectrophotometer. A fine powder of [Fe(TPP)(NO)][68,69] (37 mg) diluted with BN (∼50 mg) was pressed into a pellet and sealed between 63.5-μm Mylar windows in a 1-mm Al spacer. Iron K-edge X-ray absorption spectra (XAS) were recorded at the Stanford Synchrotron Radiation Laboratory (SSRL) on the unfocused multipole wiggler beamline 7−3 under dedicated ring conditions (3 GeV, 50−100 mA), using a Si(220) double-crystal monochromator detuned 50% (at 8257, 7993, and 8257 eV for $Mb^{III}NO$, $Mb^{II}NO$, and [Fe(TPP)(NO)], respectively). Data were collected as fluorescence spectra using a 13-element Ge array detector (proteins)[70] or with N_2-filled ionization chambers in transmission mode ([Fe(TPP)(NO)]) and were averages of multiple scans (27 for $Mb^{III}NO$, 24 for $Mb^{II}NO$, 3 for [Fe(TPP)(NO)]) measured from 6790 to 8257, 7993, and 8257 eV, respectively. The data for the proteins were collected from two different frozen samples at two spots on each sample to minimize the effects of photodecomposition. Solutions were syringed into 140-μL Lucite cells (23 × 2 × 3 mm) with 63.5-μm Mylar tape windows in a N_2-filled glovebag and then were frozen (liquid N_2/*n*-hexane). A constant temperature (10 K) was maintained using an Oxford Instruments continuous-flow liquid He CF 1208 cryostat. The energy was calibrated using an Fe foil standard (first inflection point, 7111.2 eV).[71]

The model-fitting calculations were performed using the XFIT program[72] and models and procedures described previously (Supporting Information, Figure S1).[73] The only exception was for the [Fe(TPP)(NO)] model structure, where a refinement was run in which the α carbons of the phenyl substituents were included in addition to those contained in the porphyrin ring. The positions of these carbons were obtained from the X-ray crystal structure,[69] and the following restraints were applied: C^H-C^{Ph} = 1.50 Å{0.05 Å} and $C^1-C^H-C^{Ph}$ = 118°-{2°}. The XAFS structures thus obtained probe the environment around the Fe atom with higher precision and accuracy than is possible from protein crystallography,[74,75] yielding distances accurate to 0.01−0.02 Å.[75] Moreover, the ab initio MS calculations involve significant contributions from pathways involving atoms up to 5 Å from the Fe center, which include all core porphyrin and exogenous ligand atoms for the proteins.[76] These processes are important in determining the XAFS of the distant shells and become particularly important at low *k* values or when three atoms are approximately collinear,[77] but drop off very rapidly for intervector angles smaller than ca. 150°.

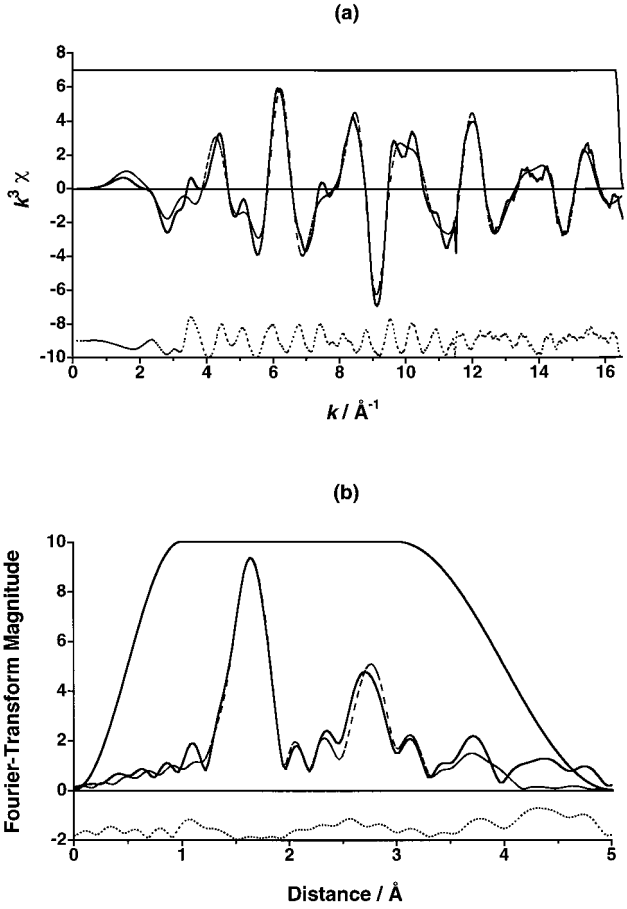

Figure 1. (a) XAFS and (b) Fourier transform amplitude of XAFS of [Fe(TPP)(NO)]: observed (—), calculated from refined model (- - -), residual (····), window used in Fourier filter (—).

Results

[Fe(TPP)(NO)]. The observed and calculated XAFS, $\chi(k) \times k^3$, the corresponding Fourier transforms, the residuals, $\Delta[\chi(k) \times k^3]$, and the window functions used in the Fourier filter for [Fe(TPP)(NO)] are shown in Figure 1, using the same model as that for the proteins excluding the axial imidazole ring. When the α carbons of the phenyl substituents are included in the

(65) Guss, J. M.; Bartunik, H. D.; Freeman, H. C. *Acta Crystallogr., Sect. B* **1992**, *B48*, 790−811.

(66) Concentrations of Mb were estimated spectroscopically for met-Mb in 0.1 M phosphate buffer (pH 6.8) using the molar absorptivities: $\epsilon_{280} = 3.37 \times 10^4\ M^{-1}\ cm^{-1}$; $\epsilon_{408} = 1.6 \times 10^5\ M^{-1}\ cm^{-1}$; $\epsilon_{505} = 1.02 \times 10^4\ M^{-1}\ cm^{-1}$. *Handbook of Biochemistry and Molecular Biology*, 3rd ed.; CRC Press: Boca Raton, FL, 1976; Vol. II (Proteins).

(67) (a) Tsubaki, M.; Yu, N.-T. *Biochemistry* **1982**, *21*, 1140−1144. (b) Mackin, H. C.; Benko, B.; Yu, N.-T.; Gersonde, K. *FEBS Lett.* **1983**, *158*, 199−202.

(68) [Fe(TPP)(NO)] was synthesized according to the literature method,[69] and the crystal structure on the sample used here was reanalyzed by Dr. Peter Turner and gave the same bond lengths and angles.

(69) Scheidt, W. R.; Frisse, M. E. *J. Am. Chem. Soc.* **1975**, *97*, 17−21.

(70) Cramer, S. P.; Tench, O.; Yocum, M.; George, G. N. *Nucl. Instrum. Methods. Phys. Res.* **1988**, *A266*, 586−591. The data for the Fe(III) adduct were obtained with a more modern detector, which could take up to 150 000 counts.

(71) Zhang, Y.; Pavlosky, M. A.; Brown, C. A.; Westre, T. E.; Hedman, B.; Hodgson, K. O.; Solomon, E. I. *J. Am. Chem. Soc.* **1992**, *114*, 9189−9191.

(72) Ellis, P. J.; Freeman, H. C. *J. Synchrotron Radiat.* **1995**, *2*, 190−195. This program incorporates FEFF 6.01 for MS (Rehr, J. J.; Albers, R. C.; Zabinsky, S. I. *Phys. Rev. Lett.* **1992**, *69*, 3397−3400).

(73) Rich, A. M.; Armstrong, R. S.; Ellis, P. J.; Freeman, H. C.; Lay, P. A. *Inorg. Chem.*, in press.

(74) Chance, M. R.; Parkhurst, L. J.; Powers, L. S.; Chance, B. *J. Biol. Chem.* **1986**, *261*, 5689−5692.

(75) Gurman, S. J. *J. Synchrotron Radiat.* **1995**, *2*, 56−63.

(76) Pin, S.; Alpert, B.; Congiu-Castellano, A.; Longa, S. D.; Bianconi, A. *Methods Enzymol.* **1994**, *232* (Hemoglobins, Part C), 266−292.

(77) Teo, B.-K. *J. Am. Chem. Soc.* **1981**, *103*, 3990−4001. Teo, B.-K. Bond-Angle Determination by EXAFS: A New Dimension. In *EXAFS and Near Edge Structure*; Bianconi, A., Inoccia, L., Stipcich, S., Eds.; Springer-Verlag: Berlin and Heidelberg, 1983; pp 11−21.

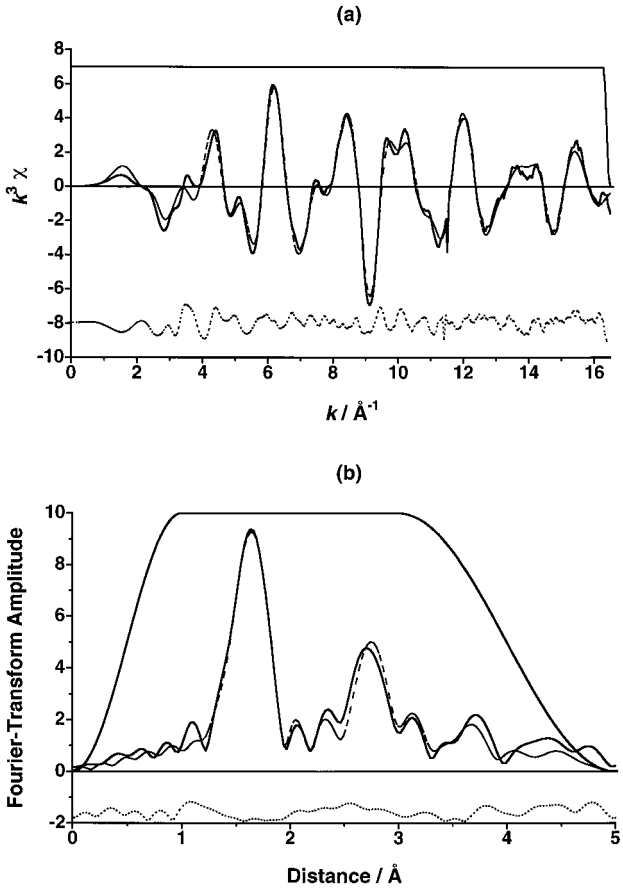

Figure 2. (a) XAFS and (b) Fourier transform amplitude of XAFS of [Fe(TPP)(NO)] when the α carbons of the phenyl substituents are included in the model: observed (—), calculated from refined model (- - -), residual (····), window used in Fourier filter (—).

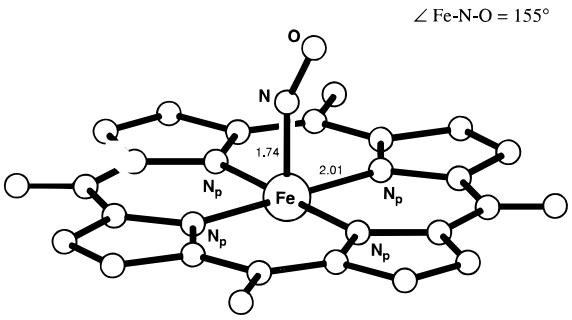

Figure 3. Molecular structure at 10 K for the non-hydrogen atoms within 5 Å of the Fe atom of [Fe(TPP)(NO)].

model (which are absent in the proteins), there is a significant improvement in the fit (Figure 2) with the *R* value decreasing from 14.2% to 12.7%. The inclusion of these extra carbons only affected the fit to the second and subsequent shells and did not have a significant effect on the Fe−ligand bond lengths and the Fe−N−O bond angle that were determined from the MS analysis. The structure of [Fe(TPP)(NO)] from the MS refinement is shown in Figure 3. The Fe−N_p(av) and Fe−N_{NO} bond distances found in the MS analysis are effectively the same as those determined from the SS analysis (Table 1). All bond lengths for the SS, MS, and crystal structure analyses were the same within experimental error. The use of MS instead of SS to analyze the XAFS data enabled the determination of the Fe−N−O angle (155°). Despite the small error (2°) in this value, the angle is somewhat larger than that determined from the crystal structure (149.2°). This discrepancy could arise from

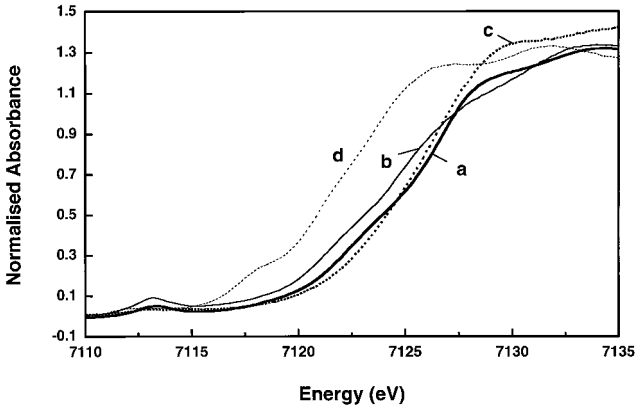

Figure 4. Edge spectra obtained at 10 K of (a) $Mb^{III}NO$ compared with those of (b) $Mb^{II}NO$, (c) met-Mb, and (d) deoxy-Mb.

differences in temperature (XAFS and crystal structure data were collected at 10 and 293 K, respectively).

X-ray Photodamage Effects on $Mb^{III}NO$ and $Mb^{II}NO$. The edge spectrum of $Mb^{III}NO$ was sensitive to irradiation. The effect was negligible during the first three to five scans but became appreciable in subsequent scans. When data for all 27 scans (five to eight scans in each of two positions for two Mb^{III}-NO samples) were averaged, there was a shift in the edge to lower energy by 0.2 eV. The nature of the photodamaged product is not known; however, the position of the edge shifts to lower energies than the corresponding edge of $Mb^{II}NO$ (edge shifts, ΔE, of up to 0.4 eV were observed for $Mb^{III}NO$, cf. $\Delta E = 0.2$ eV between the first scans of $Mb^{II}NO$ and $Mb^{III}NO$). The model was fitted to the average of 15 scans that were least affected (individual scans with an edge shift of >0.16 eV were rejected).

Figure 4 illustrates the edge spectrum of $Mb^{III}NO$ compared with those of $Mb^{II}NO$, met-Mb[73] and deoxy-Mb.[73] The edge position of $Mb^{III}NO$ is very similar to that of the ferrous nitrosyl adduct. The shift in the edge spectrum of $Mb^{II}NO$ was negligible (average shift to higher energy by 0.1 eV during data collection of 26 scans). Since the edge shifts were very small, all 26 scans were used in the analysis.

MS XAFS of $Mb^{II}NO$ and $Mb^{III}NO$. The observed and calculated MS XAFS, the corresponding Fourier transforms, the residuals, and the window functions used in the Fourier filters of $Mb^{II}NO$ and $Mb^{III}NO$ are shown in Figures 5 and 6, respectively. The corresponding heme structures are given in Figure 7. Table 1 summarizes the results together with crystallographic and XAFS results from the literature on related model compounds and proteins.

The good agreement in the coordination geometries determined by X-ray and MS XAFS for [Fe(TPP)(NO)] gives confidence in the results obtained from the MS analyses of the XAFS of the hemeproteins. For $Mb^{II}NO$, the MS analysis gave Fe−N_p(av) as 2.00 Å, Fe−N_ϵ 2.05 Å, and Fe−N_{NO} 1.75 Å and the Fe−N−O angle as 150° (R = 14.6%), all of which are in good agreement with the results obtained from the MS XAFS analysis of [Fe(TPP)(NO)] and X-ray crystal structures of [Fe(TPP)(NO)],[69] [Fe(TPP)(NO)(1-MeIm)],[78] and $Lb^{II}NO$.[45] Similarly, the bond lengths and angles obtained from the MS analysis of $Mb^{III}NO$ are in close agreement with XRD values obtained from the crystal structures of $[Fe(OEP)(NO)]^+$ and $[Fe(TPP)(NO)(OH_2)]^+$.[79] The resulting Fe−L bond lengths and angles

(78) Scheidt, W. R.; Piciulo, P. L. *J. Am. Chem. Soc.* **1976**, *98*, 1913−1919.
(79) Scheidt, W. R.; Lee, Y. J.; Hatano, K. *J. Am. Chem. Soc.* **1984**, *106*, 6, 3191−3198.

Table 1. Comparison of Fe−Ligand Bond Lengths and Angles in $Mb^{II}NO$ and $Mb^{III}NO$ Obtained from MS XAFS Analyses with Those Determined from Other XAFS Analyses or X-ray Crystal Structure Data

species	method	Fe−Ligand distances (Å)				av Fe−N[a] (Å)	Fe−N−O angle (deg)	Debye−Waller factors, σ^2 (Å^2)				other refinement parameters		
		N_p	N_ϵ/OH_2/S	N_{NO}	N−O			N_p	N_ϵ	N_{NO}	O_{NO}	E_0 (eV)	S_0^2	R (%)
$Mb^{II}NO$	SS[b]	2.02(2)		1.76(6)	−	2.02	−							
	MS[c,d]	1.99(2)	2.05(3)	1.76(2)	1.12(2)	2.00	150(2)	0.002	0.001	0.005	0.005	7125.0	0.865	13.8
	MS[c,e]	2.00(2)	2.05(3)	1.75(2)	1.12(2)	2.01	150(2)	0.002	0.001	0.005	0.005	7125.2	0.859	14.6
	crystal[f]	2.07_7	2.18(3)	1.89(4)	1.15	2.09_7	112							
$Lb^{II}NO$	crystal[g]	1.99(7)	2.20(7)	1.72(7)	1.35[h]	2.03	147(4)							18.4
$Hb^{II}NO$	crystal[i]	−	−	1.74	1.1	−	145(10)							−
Cyt *c* peroxidase (NO)	crystal[j]	−	2.04	1.82			125, 135							
[Fe(TPP)(NO)]	crystal[k]	2.001(3)	−	1.717(7)	1.12(1)	2.00	149.2(6)							6.1
	MS[c]	2.01(2)	−	1.74(2)	1.12(2)	2.01	155(2)	0.003	−	0.005	0.007	7126.8	0.991	14.2
	MS[c,l]	2.00(2)	−	1.73(3)	1.12(2)	2.00	156(2)	0.003	−	0.005	0.007	7126.3	0.970	12.7
[Fe(TPP)(NO)(1-MeIm)]	crystal[m,n]	2.008(4)	2.180(4)	1.743(4)	1.121(8)	2.04	142.1(6)							7.4
					1.14(1)		138(1)							
$Mb^{III}NO$	MS[c,o]	2.00(2)	2.04(3)	1.68(2)	1.13(2)	2.01	180(4)	0.001	0.001	0.006	0.006	7128.8	0.946	14.3
P450nor-NO	MS[p]	2.00(2)	2.26(2)	1.66(2)			170(10)							
P450cam-NO	MS[p]	2.00(2)	2.26(2)	1.76(2)			170(10)							
$[Fe(TPP)(NO)(OH_2)]^+$	crystal[q,r]	1.999(6)	2.001(5)	1.652(5)	1.150	2.00	174(1)							7.9
$[Fe(OEP)(NO)]^+$	crystal[q,s]	1.994(3)	−	1.644(3)	1.112(4)	1.99	176.9(3)							6.3

[a] The average Fe−N distance includes the four Fe−N_p's and Fe−N_ϵ, if applicable. [b] The Fe−N_p and Fe−N_ϵ bonds were not distinguished in the SS analyses.[43] [c] This work. Data were collected at 10 ± 1 K and were analyzed using the TPP model. Errors in E_0 and S_0^2 were 0.2 eV and 0.014, respectively. [d] Data were refined with R_{max} = 5.1 Å (R_{eff} = 10.2 Å), number of legs = 6, and no filters ∴ 285 unique paths were examined and included in the refinement. [e] Data were refined with two filters in place, so that paths contributing less than 2% relative to the strongest path are rejected ∴ 104 unique paths were included in the refinement. Errors in E_0 and S_0^2 were 0.5 eV and 0.033, respectively. [f] 1.7-Å resolution SW $Mb^{II}NO$.[48] [g] 1.8-Å resolution.[45b] Errors were estimated by analogy with the uncertainties in the M−L bond lengths for a small Cu protein as a function of resolution.[65] [h] The error estimate in L−L bond lengths is uncertain. [i] 2.8-Å resolution.[44] The structure of horse $Hb^{II}NO$ was deduced by a difference Fourier map of HbNO minus met-Hb, calculated using the refined phases of met-Hb, (Ladner, R. C.; Heidner, E. J.; Perutz, M. F. *J. Mol. Biol.* **1977**, *114*, 385−414); hence, *R* was not reported; error in Fe−N_{NO} bond length is estimated to be at least 0.2 Å. Deatherage and Moffat[44] estimate the error in ∠Fe−N−O to be ±10°. [j] Reference 46. [k] Distances and angles obtained from ref 69. Data were collected at 293 K. [l] Model included the α carbons of the phenyl substitutents. [m] Distances and angles obtained from ref 78. Data were collected at 293 K. [n] The two angles represent the major and minor orientations of the nitrosyl oxygen; the occupancy factors of the oxygen atoms were 0.67(3) and 0.32(2), respectively. [o] 15-scan average; 105 unique paths included in the refinement. Errors in E_0 and S_0^2 were 0.2 eV and 0.014, respectively. [p] P450nor refers to the nitric oxide reductase (nor) enzyme from *Fusarium oxysporum*, which has been designated as a cytochrome P450 system because of its similarity to this class of enzymes. P450cam refers to the *d*-camphor-bound form of cytochrome P450 from *Pseudomonas putida*.[47] [q] Scheidt et al.[79] [r] Data were collected at 96 K. [s] Data were collected at 292 K.

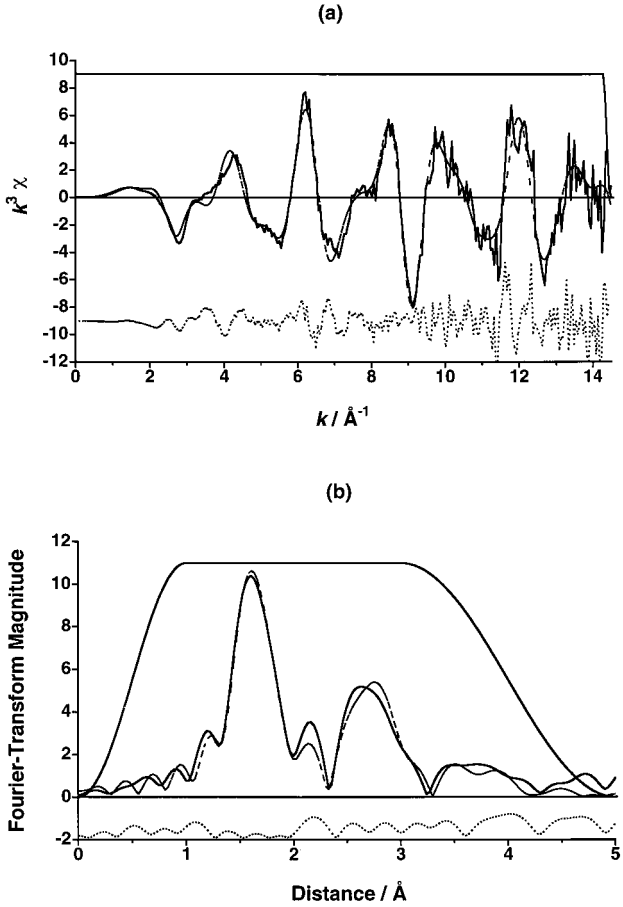

Figure 5. (a) XAFS for $Mb^{II}NO$: observed (—), calculated from refined model (- - -), residual (••••), window used in Fourier filter (—). (b) Fourier transform amplitude of XAFS for $Mb^{II}NO$: observed (—), calculated from refined model (- - -), residual (••••), window used in Fourier filter (—).

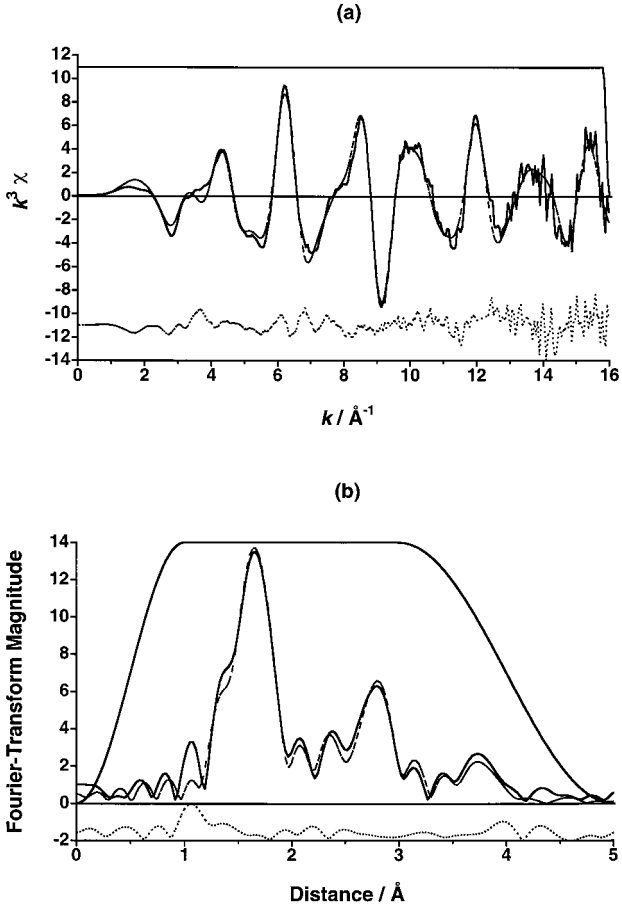

Figure 6. (a) XAFS for $Mb^{III}NO$: observed (—), calculated from refined model (- - -), residual (••••), window used in Fourier filter (—). (b) Fourier transform amplitude of XAFS for $Mb^{III}NO$: observed (—), calculated from refined model (- - -), residual (•••), window used in Fourier filter (—).

for both the 15-scan and 27-scan averages were the same within experimental error. Therefore, the small amount of photodamage averaged over all of the scans for $Mb^{III}NO$ did not result in a significant change in bond lengths. This is reflected in the E_0 value: a 0.6-eV decrease in E_0 resulted in a 0.005-Å decrease in Fe−N_{NO}.[80] The small R value (14.3%) and the correspondence of the model complexes with the protein again give confidence in the accuracy of the XAFS-derived structure.

Effect of Varying N−O on the Fe−N−O Angle in Ferrous and Ferric MbNO. To determine the effect of varying the N−O bond distance on the Fe−N−O angle in ferrous and ferric MbNO, refinements were performed where this restraint was lowered or raised by 0.01 Å (Table S1, Supporting Information). A variation of ±0.02 Å in the N−O distance used in the refinement of the structure derived from the XAFS of $Mb^{II}NO$ results in a variation of 2.2° in the Fe−N−O angle. Hence, if the estimated standard deviation (esd) in the N−O bond distance is 0.01 Å, then the esd in the Fe−N−O angle is 1.1°. In the refinement of $Mb^{III}NO$, a variation of the N−O distance by ±0.01 Å results in a 4.8° difference and, thus, an esd of 2.4° in the Fe−N−O angle. These esd values were used in calculating the overall estimate of the root-mean-square (rms) error in ∠Fe−N−O.

Accuracy and Precision in Fe−L Bond Lengths and the Fe−N−O Angle from XAFS. Monte Carlo calculations of error due to noise in the data yielded rms errors for [Fe(TPP)(NO)] of 0.001 Å for Fe−N_p, 0.002 Å for Fe−N_{NO}, and 0.86° for ∠Fe−N−O. The respective errors estimated for $Mb^{II}NO$ and $Mb^{III}NO$ were 0.004 and 0.002 Å for Fe−N_p, 0.004 and 0.003 Å for Fe−N_ϵ, and 0.010 and 0.003 Å for Fe−N_{NO}. These statistical errors were combined with typical systematic errors (±0.01−0.02 Å)[75] to obtain the estimated maximum rms errors in the reported bond lengths (Table 1).

Monte Carlo calculations yielded respective rms errors of 2.1° and 2.8° for the Fe−N−O bond angles in $Mb^{II}NO$ and Mb^{III}-NO, which were combined with the rms errors of 1.1° and 2.4°, resulting from varying the N−O distance (Table S1, Supporting Information), to give estimated maximum rms errors of 2.4° and 3.7°, respectively.[83]

Effect of Varying Fe−N_ϵ on the Fe−N−O Angle in $Mb^{II}NO$. Some test refinements were performed to determine the effect of varying the Fe−N_ϵ bond length on the derived Fe−N−O angle and Fe−N_{NO} bond distance in HH $Mb^{II}NO$. The Fe−N_ϵ bond distance was increased from 1.96 to 2.30 Å in 0.02-Å increments. The parameters refined included all Debye−Waller temperature factors, positional coordinates for all atoms except the N_ϵ coordinates, E_0, and S_0^2 (Table S2,

(80) This observed decrease is consistent with the estimation of a ±0.005 Å change in Fe−L for every 1-eV change in E_0.[81,82]

(81) Ellis, P. J. Ph.D. Thesis, University of Sydney, 1995.

(82) Penner-Hahn, J. E.; Hodgson, K. O. In *Iron Porphyrins, Part III*; Lever, A. B. P., Gray, H. B., Eds.; VCH Publishers: New York, 1989; Vol. 4, Chapter 3 and references therein.

(83) Estimate of rms error in the Fe−N−O angle for $Mb^{II}NO$: error in ∠Fe−N−O = $[(1.1°)^2 + (2.1°)^2]^{1/2}$ = 2.4°. Estimate of rms error in the Fe−N−O angle for $Mb^{III}NO$: error in ∠Fe−N−O = $[(2.4°)^2 + (2.8°)^2]^{1/2}$ = 3.7°.

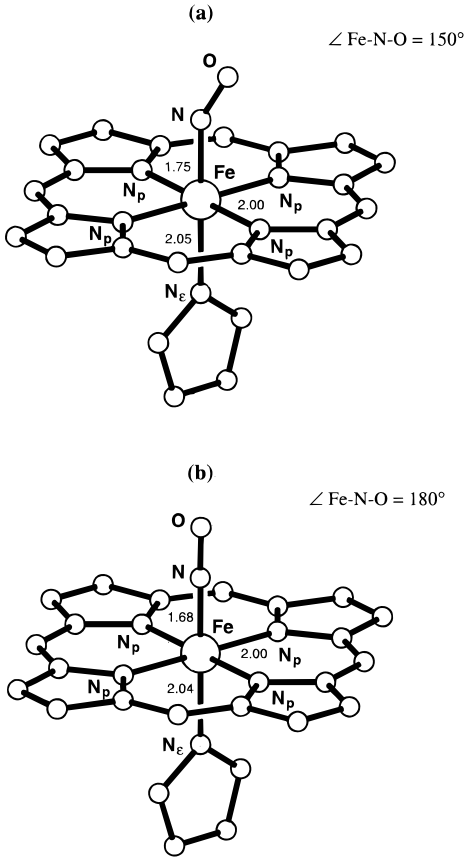

Figure 7. Molecular structures (determined at 10 K) for the non-hydrogen atoms within 5 Å of the Fe atom of (a) $Mb^{II}NO$ and (b) Mb^{III}-NO at 10 K.

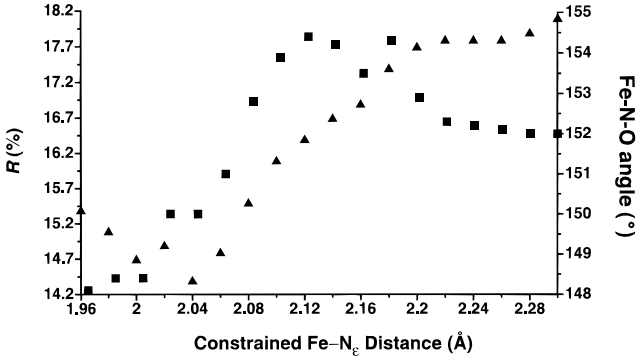

Figure 8. MS XAFS analyses of HH $Mb^{II}NO$ with a constrained Fe−N_ϵ distance: effect on the residual, R (▲), and the Fe−N−O angle (■) as a function of distance.

Supporting Information). There were no significant changes in the Fe−N_{NO} bond distance in the refinements. The changes in the resulting Fe−N−O bond angles, relative to the minimum obtained without constrained or restrained Fe−L bond lengths, ranged from +4.3° to −2° (Figure 8). The best refinement resulted from an Fe−N_ϵ bond distance of 2.04 Å (R = 14.4%), which corresponds to the original minimum.

Refinements with Restrained Fe−N−O Bond Angles. Refinements were performed where the Fe−N−O angle was tightly restrained to be 109°, 115°, 120°, 125°, 130°, 140°, 160°, or 170° (σ_{res} = 1°) for $Mb^{II}NO$; and 109°, 120°, 130°, 140°, 150°, 160°, or 170° (σ_{res} = 1°) for $Mb^{III}NO$, to determine whether another minimum could be detected. These restraints were then removed, and the data were re-refined (Tables S3 and S4, Supporting Information). For $Mb^{II}NO$, when the initial bond angle was 109°−120°, the Fe−N−O angle refined to an angle of 120° after restraints were removed. For 125°, the angle remained at 125° after the restraints were removed, whereas for angles of 130° or higher, the Fe−N−O angle refined to an angle of 150°. However, the R values for the minima where Fe−N−O refined to an angle of 120° or 125° are 0.6% and 2.1% higher, respectively, than that where the angle refined to 150°. In the refinements with Fe−N−O restraints, the bond lengths did not deviate significantly from those obtained from the true minimum. However, the Fe−N−O bond angles differed significantly due to the tight restraints. The further the angle was restrained from the global minimum, the higher was the R factor for angles of 130° or higher (130°, R = 16.7%; 170°, R = 15.5%). Hence, MS XAFS analysis can distinguish Fe−N−O angles between 130° and 170°.

For $Mb^{III}NO$, the fit obtained when low initial angles were used (109°−130°) and the restraints were released was a false minimum. For this minimum, an Fe−N−O angle of 122° was obtained, but the R value was 4.9% higher than for the structure of best fit (Fe−N−O angle of ∼180°) obtained from higher starting angles. In the refinements with Fe−N−O restraints, the bond lengths did not deviate by more than 0.03 Å from those obtained from the true minimum, but the Fe−N−O bond angle differed significantly. However, the refinements where the restraint was far from the true value (e.g., 140°) resulted in Fe−N−O angles that did not "obey" the restraint, although σ_{res} was 1°. This was reflected in the refinement parameters, since the further the angle deviated from the minimum, the higher the S_0^2 and R factors (140°: S_0^2 = 1.09, R = 18.6%; 150°: S_0^2 = 1.04, R = 15.6%) were. The values of the S_0^2 and R factors decrease as the restraining angle approaches the ideal value of 180°. This confirms the sensitivity of the MS XAFS analysis to the Fe−N−O bond angles. The results show that MS analyses of XAFS data are capable of determining Fe−N−O bond angles in hemeproteins and that the major differences between the structures of $Mb^{III}NO$ and $Mb^{II}NO$ lie in the Fe−N_{NO} bond lengths and Fe−N−O bond angles.

To test further the validity of the above analyses, MS refinements were performed where the Fourier transform XAFS window was limited to include only the peak due to the Fe−N−O angle (∼2.0−2.3 Å window). The Fe−N−O angle was restrained to values ranging from 109° to 180° and the XAFS data were refined. The R values plotted as a function of Fe−N−O angle are illustrated in Figures 9 (for the proteins) and S2 (for [Fe(TPP)(NO)]). From these results, the Fe−N−O moiety is bent in ferrous $Mb^{II}NO$ and [Fe(TPP)(NO)], while in the ferric nitrosyl complex, the angle is close to being linear.

Similar calculations were performed on the XAFS data obtained for [Fe(TPP)(NO)] to test the effect of the axial imidazole group of the proteins in causing a false minimum (Table S5, Supporting Information). A second minimum with an Fe−N−O angle of ∼120° was also observed (Figure S2), but this was not as deep as that for $Mb^{II}NO$.

Can MS Distinguish Fe−N_p from Fe−N_ϵ? The MS XAFS analyses of $Mb^{II}NO$ and $Mb^{III}NO$ result in similar Fe−N_p and Fe−N_ϵ bond lengths (Table 1). The bond distances differ by only 0.05 and 0.04 Å in $Mb^{II}NO$ and $Mb^{III}NO$, respectively. Since the rms error estimates are 0.02 and 0.03 Å for Fe−N_p and Fe−N_ϵ, respectively, these differences may be insignificant. To determine whether MS can distinguish between these two bonds, refinements were performed where the five Fe−N_p and Fe−N_ϵ bond lengths were constrained to be identical (Table S6, Supporting Information). In both $Mb^{II}NO$ and $Mb^{III}NO$, the Fe−N_{av} and Fe−N_{NO} bond lengths and Fe−N−O angles are the same as those determined in the original refinements,

within the errors of the analyses. The residual, *R*, increased by 0.6% when the Fe−N_p and Fe−N_ϵ bond lengths were constrained to be identical. However, when these constraints were removed, the bond lengths and angles reverted to their original values. While, it is uncertain whether the MS analysis can resolve the Fe−N_p and Fe−N_ϵ bond lengths, one distinguishing feature of the Fe−N_p and Fe−N_ϵ bonds is the contributions of the methine carbons of the porphyrin to the MS analysis. The Fe → C(methine) → Fe path, which is absent from the imidazole, has a SS importance factor (26%) that is the same as that due to the SS Fe → N_ϵ → Fe path (26%) as outlined in the Supporting Information (Table S7). This SS contribution, together with the MS contributions involving the methine carbons, is likely to be the reason the two Fe−N bond lengths are differentiated in the MS pathways when restraints are removed. The limited XAFS resolution of SS analyses cannot resolve such bond lengths.[84] Irrespective of whether these refinements (and the refinements illustrated in Figure 8) resolve the two bond lengths, it is evident that they are similar and that the results are inconsistent with substantial axial elongation of the Fe−N_ϵ bond.

Are Four- and Five-Leg MS Paths Important in the Analysis of MbNO? MS paths up to five legs with total distances $R \leq 5$ Å[85] were incorporated into the refinements of the XAFS data. Of the 104 MS paths incorporated into the refinement of $Mb^{II}NO$ (Table S7, Supporting Information), 20 involve five legs. The most significant five-leg path, Fe → C^{1D} → N^D → C^{1D} → N^D → Fe, has an importance factor of 16% relative to the strongest paths and an *R* value of 4.6 Å. To determine the significance of these five-leg paths, refinements of $Mb^{II}NO$ and $Mb^{III}NO$ were repeated where paths up to four legs only were included in the calculation (Table S8, Supporting Information). The resulting calculations included 84 and 83 paths for $Mb^{II}NO$ and $Mb^{III}NO$, respectively (cf. 104 and 105 paths in the corresponding five-leg calculations). The Fe−L bond lengths and Fe−N−O angles determined from the four-leg refinements were the same as those derived using up to five legs within the error estimates of the MS analyses. Thus, the arbitrary inclusion of five-leg MS paths is insignificant with respect to the Fe−L bond lengths and Fe−N−O angles obtained. It does, however, cause a significant effect on the correspondence between the observed and calculated XAFS, although this is manifested mainly at low *k* values and in the second and subsequent shells of the Fourier transform (Figure 10). When the XAFS contributions of two-, three-, and four-leg paths involving the NO ligand to the MS are compared (Figures S3 and S4), it is clear that paths up to four legs make significant contributions to the XAFS.

Discussion

[Fe(TPP)(NO)]. The Fe−N_p(av) and Fe−N_{NO} distances in [Fe(TPP)(NO)] are within experimental error of the bond lengths determined by X-ray crystallography. The bond angle of 155° is 6° larger than that determined by X-ray crystallography; however, they are almost the same within experimental error. It is unclear if the different temperatures of the determinations or the NO disorder in the crystal structure[69] may contribute to these differences. Nonetheless, the coordination geometries determined by X-ray and MS XAFS are in good agreement and give confidence as to the XAFS analyses of the proteins.

(84) Riggs-Gelasco, P. J.; Stemmler, T. L.; Penner-Hahn, J. E. *Coord. Chem. Rev.* **1995**, *144*, 245−286 and references therein.

(85) *R* is half the effective path length, which is the length of the route by which a photoelectron proceeds from the absorber to neighboring atoms and back to the absorber.

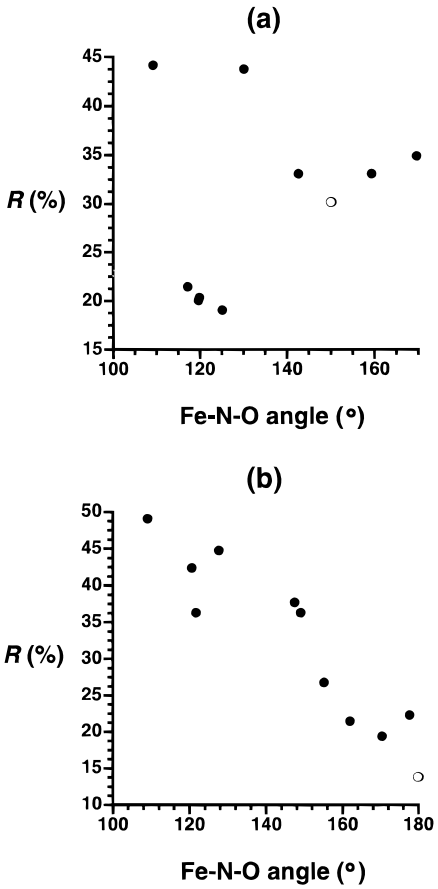

Figure 9. MS XAFS analyses of HH (a) $Mb^{II}NO$ and (b) $Mb^{III}NO$ using a Fourier transform windowed from ∼2.0−2.3 Å. The closed circles correspond to calculations where the Fe−N−O angle was restrained and the Fourier transform peak due to this angle was refined. The open circles correspond to the minimum obtained when no restraints were applied to the Fe−N−O angle.

The results also show that quite distant carbons can have a significant contribution to the XAFS at low *k* values. This is shown by the importance of the α carbons of the phenyl substituents, which are 4.9 Å away from the Fe center. The inclusion of such contributions decreases the *R* factor by 1.5% due to the 4-fold degenerate SS pathway and the 8-fold degenerate linear MS pathway involving the meso carbons.

$Mb^{II}NO$ and $Mb^{III}NO$. For $Mb^{II}NO$, values of the bond lengths and angles (Fe−N_p(av), 2.00 Å; Fe−N_ϵ, 2.05 Å; Fe−N_{NO}, 1.75 Å; Fe−N−O angle, 150°) are consistent with X-ray crystal and MS XAFS structures of the model complexes, [Fe(TPP)(NO)] and [Fe(TPP)(NO)(1-MeIm)], and the crystal structures of $Hb^{II}NO$[44] and $Lb^{II}NO$.[45] The angle is also consistent with the angle of 153° deduced from room-temperature EPR experiments but is inconsistent with the much smaller value of 109° that has been deduced from EPR measurements at 77 K[53] and the angle of 112° determined in the 1.7-Å resolution XRD structure of SW $Mb^{II}NO$.[48] It is clear from Table S3 that such a small angle cannot be accommodated while retaining a reasonable fit to the XAFS data. Such a restraint results in an increase in the *R* factor by 2.2% and a 5-fold increase in the Debye−Waller factor for the terminal oxygen of the NO ligand, compared to that obtained for the structure of best fit. It is not clear why the low-temperature EPR and the XRD values determined for the Fe−N−O angle are inconsistent with all of the other structural and room-temperature EPR data on Fe^{II}−NO heme adducts, but this may be a result of the way in which they were prepared. As pointed out by Phillips, the distal

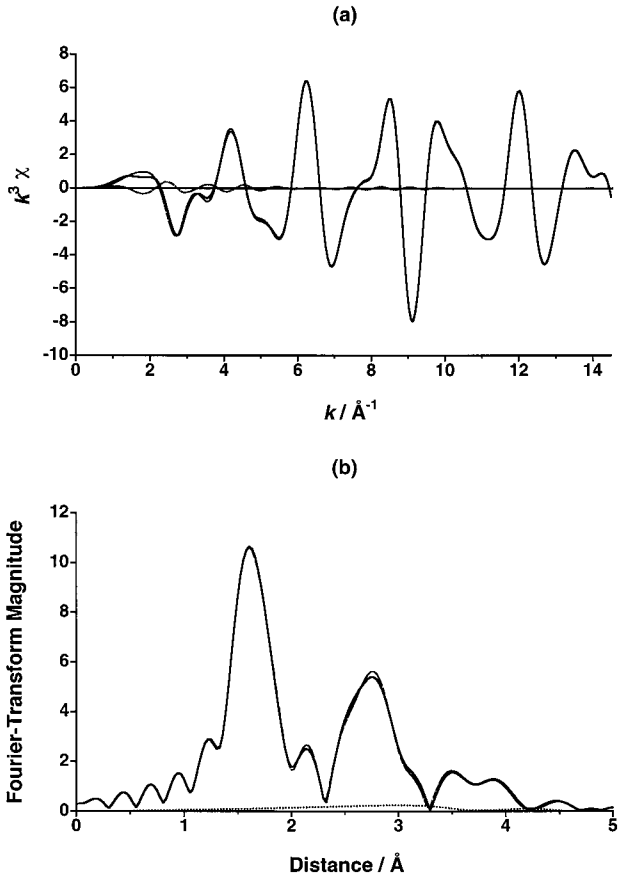

Figure 10. (a) Calculated XAFS and (b) Fourier transform amplitude of the calculated XAFS of HH Mb^{II}NO: two- to five-leg paths (—), two- to four-leg paths (- - -), five-leg paths (•••).

histidine in the crystals of met-Mb used to prepare the Mb^{II}NO crystals is hydrogen-bonded to the aqua ligand in met-Mb.[48] This forces the NO to adopt a small angle when it replaces the aqua ligand in the crystal structure. These packing forces do not necessarily apply when the NO adduct is prepared in aqueous solutions, as was the case for the XAFS experiments reported here, where the adduct appears to adopt a more normal bonding angle. It is clear that the aqueous preparative method is more biologically relevant than substitution in and reduction of crystals, and hence, we believe that the XAFS structure is likely to be that adopted in vivo when Mb reacts with NO.

The false minima in the fit to the data can be explained readily by considering the degenerate Fe−N$_\epsilon$−C$_\alpha$ and Fe−N$_p$−C$_m$ angles of 127.6° and 127.0°, respectively. These angles are close to the second minimum at 125.1° found in the plot of the Fe−N−O angle versus *R* for the second shell (Figure 9a). Several pieces of evidence point to the deduction that this value does not correspond to the actual Fe−N−O angle. The first is that, when all MS paths are considered, the *R* factor is 2.1% higher when the angle is restrained to 125° compared to the true minimum at 150°. The second is that the Debye−Waller factor for the terminal O of the NO group is a factor of 20 higher when the angle is 125° versus 150°. This large Debye−Waller factor is to be expected if the Fe−N−O moiety is being treated in the fit as an Fe−N−C moiety. A similar explanation may apply to the other false minimum at 120°. If the explanation for the minima around 120° were correct, then similar but more shallow minima around 120° would be expected for both [Fe(TPP)(NO)] and Mb^{III}NO. The fact that this was found in the analysis strengthens the arguments outlined above. In the case of [Fe(TPP)(NO)], the lack of an axial imidazole means that there are fewer Fe−N−C angles of 120−130°, and hence, the Fe−N−O angle is more easily distinguished from the Fe−N−C angles than in Mb^{II}NO. For Mb^{III}NO, the nearly linear Fe−N−O moiety results in much larger MS contributions than for the same moiety in the Fe(II)−NO adducts, and hence, it is much more easily distinguished from the false minimum where it is fitted to the Fe−N−C angles.

The bond lengths and angles obtained for Mb^{III}NO are consistent with analogous bonding parameters in the crystal structures of [Fe(OEP)(NO)]$^+$ and [Fe(TPP)(NO)(OH$_2$)]$^+$.[79] The small *R* value (14.5%) and the correspondence of the model complexes with the protein both give confidence in the accuracy of the XAFS-derived structure. It is difficult to study the effects of temperature (10 K versus ambient temperature) on the bond angle information because of the instability of the Fe(III) adduct to "autoreduction" at ambient temperature.[41,67] The ability to obtain accurate and precise bond angle data at higher temperature is complicated, for both oxidation states, by increased photodamage and smaller contributions due to MS pathways because of increased thermal motion. The linear Fe−N−O moiety is also consistent with recent resonance Raman spectroscopic results and MS XAFS analysis of the NO adduct of Fe(III) in ferric hemeprotein, nitric oxide reductase.[47] In addition, the resonance Raman spectrum of Mb^{III}NO has oxidation and spin state marker bands similar to those of Mb^{II}NO,[60] suggesting that the former complex is best considered as Fe^{II}−NO$^+$,[41,61] which is consistent with the XAFS structure.

It is interesting to compare the results obtained from the current MS XAFS analysis of Mb^{III}NO and Mb^{II}NO with the only other MS XAFS analysis of NO adducts of hemeproteins (i.e., the Fe(III)−NO adducts of cyt P450nor and P450cam).[47] The latter experiments differ in at least two ways from those reported here. The first is that the experiments were performed at a higher temperature (80 K) over 8−10 h. If these proteins are anywhere near as sensitive to photoreduction as Mb^{III}NO, then such conditions would result in substantial degradation of the proteins, since we have found that even at much lower temperatures (10 vs 80 K) and shorter exposure times (3−4 h vs 8−10 h) substantial photoreduction of Mb^{III}NO occurs. Since there is no evidence in the previous publication[47] that the data were examined for photodamage to the proteins (and appropriately affected data rejected), this could lead to substantial problems in interpretation of the previous data. This is evident in the bond length data of cyt P450norNO and P450camNO where the Fe−NO bond lengths were determined to be 1.66(2) and 1.76(2) Å, respectively. While the former is consistent with all of the other Fe−NO bond lengths of Fe(III)−NO adducts contained in Table 1, the latter is typical of the bond lengths of the Fe(II)−NO adducts (1.72−1.76 Å). This is also consistent with the report that cyt P450camNO is much more easily reduced than cyt P450norNO and that the Fe−N−O bond angle for the former is smaller than for the latter. The second problem with the previous analysis is that data were only analyzed over a small *k* range (4−12.5 Å^{-1}), which makes the determination of precise bond lengths and bond angles more difficult. These, combined with the photoreduction effects, are the likely reasons for the poorly determined Fe−N−O bond angles in the previous MS XAFS analyses of NO adducts of hemeproteins. These emphasize the caution that must be taken in ensuring the integrity of such readily reduced proteins in the MS XAFS analyses of hemeproteins.

Conclusions

The results show that MS analyses of XAFS data are capable of determining Fe−N−O bond angles in hemeproteins and that the major differences between the structures of $Mb^{III}NO$ and $Mb^{II}NO$ lie in the Fe−N−O bond angles. It is clear, however, that caution is required in the selection of the starting bond angle for the Fe−N−O moiety to avoid obtaining an incorrect structure. The results also point to the care that needs to be taken in interpreting XRD and spectroscopic data based on single-crystal measurements where the NO is forced to replace a smaller ligand on the coordination site. When NO replaces OH_2 in the crowded heme pocket of met-Mb, it may force an unusual geometry on the NO binding, which would not be the case when the same adducts are allowed to form in solution free from crystal packing forces (as indicated by the XAFS results). Another potential problem with the XRD and other single-crystal measurements would be incomplete binding of NO to met-Mb. This would lead to structural inaccuracies due to the presence of the two species. In the cases of $Hb^{II}NO$ and $Lb^{II}NO$, the heme pockets are more open and similar preparative methods involving substitution reactions in crystals do not force unusual geometries on the NO bonding. From our results, it is clear that the bondings of NO to Lb, Hb, and Mb are similar and that this bent structure, with a typical angle of 140−150°, is likely to be found in a range of biologically relevant hemeproteins in vivo. In contrast to the proteins discussed here, it is not clear why the bond to the proximal histidine in GC is substantially elongated on NO binding. Finally, it is evident that four-leg paths are also important in determining the MS contributions of bound NO. In previous experiments of NO bonding to non-heme iron complexes, only paths up to three legs were considered.[64] It is not clear how these may have affected the accuracy of the previous results.

Acknowledgment. We are grateful for access to the facilities at SSRL, the Australian Nuclear Science and Technology Organisation, access to the Major Facilities Program, an Australian Postgraduate Research Award and James Kentley Memorial Traveling Scholarship (A.M.R.), and funding from the Australian Research Council (R.S.A. and P.A.L.). We thank Dr. S. Easterbrook-Smith for purification of Mb, Professor K. Hodgson and Dr. Britt Hedman for assistance at SSRL and discussion of the results, Dr. P. Turner for the X-ray structural analysis of [Fe(TPP)(NO)], Dr. Angela Maclean for donation of the [Fe(TPP)Cl], and Professor H. C. Freeman and Dr. A. Levina for helpful discussions. Work was done (partially) at SSRL, which is operated by the Department of Energy, Office of Basic Science. The SSRL Biotechnology Program is supported by the NIH, Biomedical Research Technology Program, National Center for Research Resources. Further support is provided by the Department of Energy, Office of Health and Environmental Research.

Supporting Information Available: Tables S1−S8 containing the effects of restraining the Fe−N_ϵ bond length, the Fe−N−O bond angle, the Fe−N_ϵ and Fe−N_p bond lengths to be equal, or the number of legs (four or five) on the MS XAFS analyses and the importance factors for the MS paths for the XAFS analysis of $Mb^{II}NO$ and Figures S1−S4 of the TPP model used in the calculations, the effect of restraining the Fe−N−O angle to different values in the refinement of [Fe(TPP)(NO)], and calculated XAFS and Fourier transforms for two-, three-, four-, and five-leg paths of the Fe−N−O moiety (16 pages). See any current masthead page for ordering information and Web access instructions.

JA980253G